# Image Gallery

| Clinical signs of chronic venous disease | |
|---|---|
| Image 1: Telangiectasia (C1)<br>  | Image 2: Reticular veins (C1)<br>  |
| Image 3: Varicose veins (C2)<br>  | Image 4: Oedema (C3)<br>  |

| | |
|---|---|
| Image 5: Lipodermatosclerosis (C4b)<br>  | Image 6: Corona phlebectatica (C4c)<br>  |
| Image 7: Healed ulcer (C5)<br>  | Image 8: Active ulcer (C6)<br>  |

## Image 9: Adipose tissue in the saphenous compartment.

Transverse view of the SSV at the upper calf (Left) and mid calf (right) level. There is only a small amount of adipose tissue contained within the saphenous compartment. However, the volume of adipose tissue increases towards the lower part of the calf due to gravity and orthostasis. This sonographic appearance is typically observed in women with lipedema, progressively impairing the lymphatic drainage and leading to saphenous compartment syndrome.

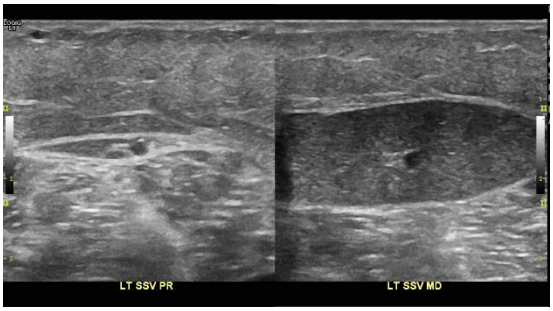


## Image 10: Egyptian eye sign.

Normal appearance of the GSV at the mid thigh, showing that saphenous vein is enclosed by the saphenous fascia and deep muscular fascia. It gives a characteristic sonographic appearance known as Egyptian eye sign.

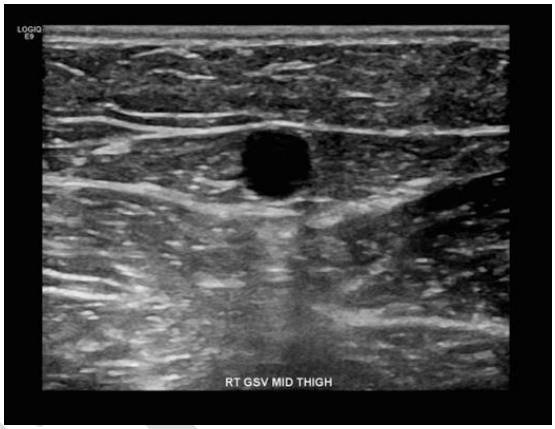


## Image 11: Colour image of the CFV.

A longitudinal view of the right CFV showing venous flow from the FV and DFV (labelled as PFV in the image) drain into the CFV. (blue: veins; red: artery)


## Image 12: Intergemellar vein.

Transverse image of the SSV at the upper calf level with an intergemellar vein coursing under the saphenous compartment between the heads of gastrocnemius muscles.

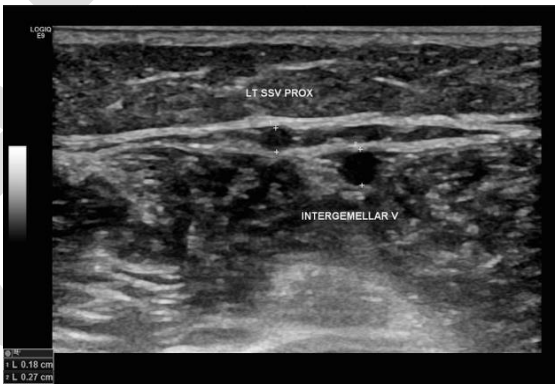


## Image 13: Duplication of the GSV.

B-mode image shows duplicated GSV at the mid thigh level with doubled veins within the saphenous compartment.


## Image 14: Hypoplasia of the GSV

B-mode image shows the hypoplasia of the GSV at the level of the distal thigh with a large epifascial tributary vein that functions as the GSV.

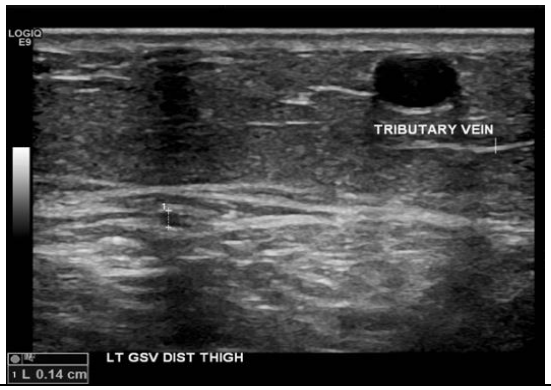

Image 15: Ultrasound image of the terminal valve (TV) and preterminal valve (PTV)

A longitudinal view of the left SFJ showing TV and PTV in the terminal section of the GSV just below its confluence with the CFV.


Image 16: Alignment sign.

Transverse image of the upper thigh shows the ASV lies on the same axis as the superficial femoral artery (SFA) and FV. This "alignment sign" allows the ASV (labelled as AAGSV in the image) to be distinguished from the GSV.

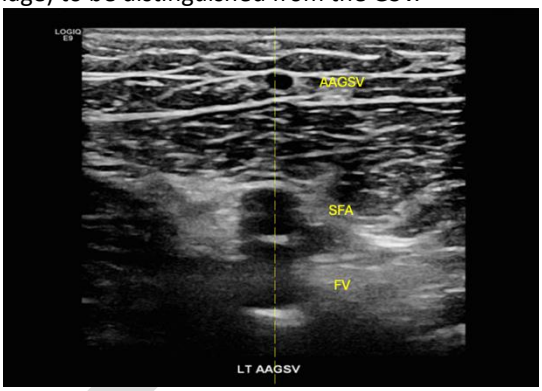


Image 17: PAGSV.

B-mode ultrasound image of the PAGSV (labelled as PASV in the image) showing its anatomical relationship with the GSV, LNVN and ASV (labelled as AASV in the image).

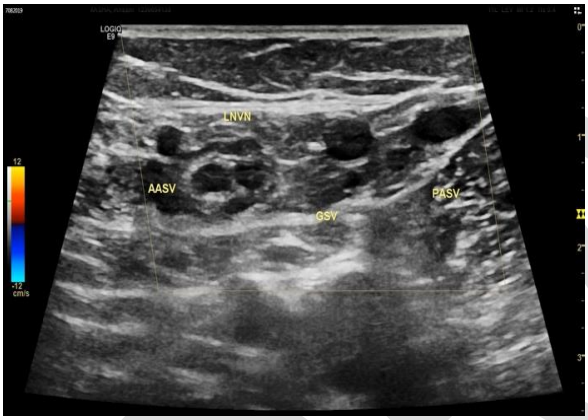


Image 18: Duplication of the SSV.

B-mode image shows duplicated SSV at the level of mid calf with both veins situated within the saphenous compartment.

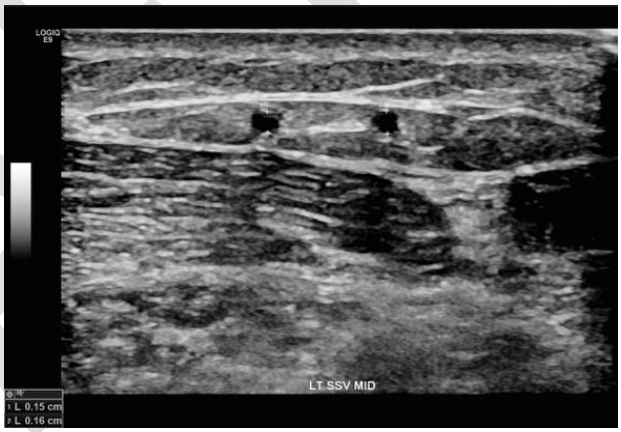


Image 19: Termination of the SSV.

B-mode image shows that the SSV and MGV join with the popliteal vein via separate junctions.

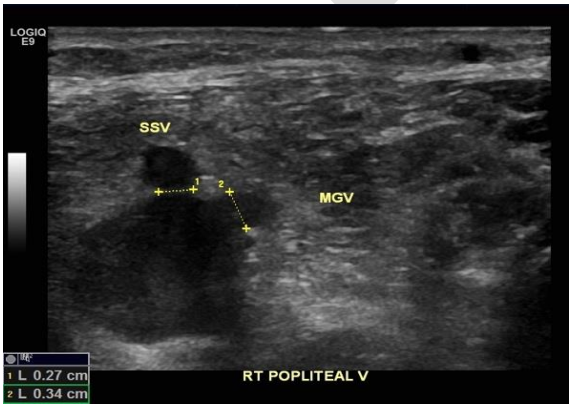


Image 20: Common trunk formed by the SSV and MGV.

Longitudinal B-mode image shows the SSV merges together with the MGV before joining the popliteal vein.

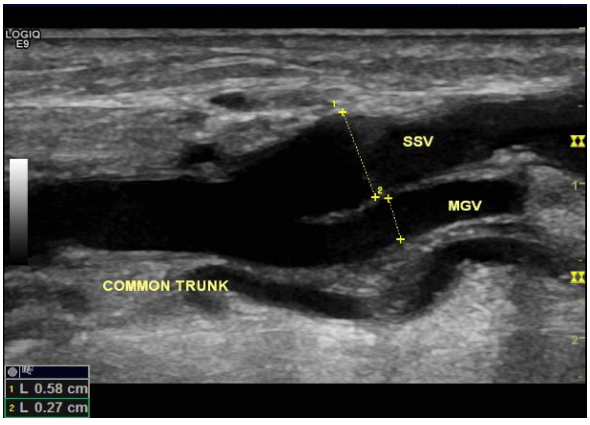

Image 21: Superficial peroneal nerve vein.
Panaramic B-mode image of the superficial peroneal nerve vein (labeled as lat SSV in the image) which is situated in its own fascial compartment in the lateral calf.

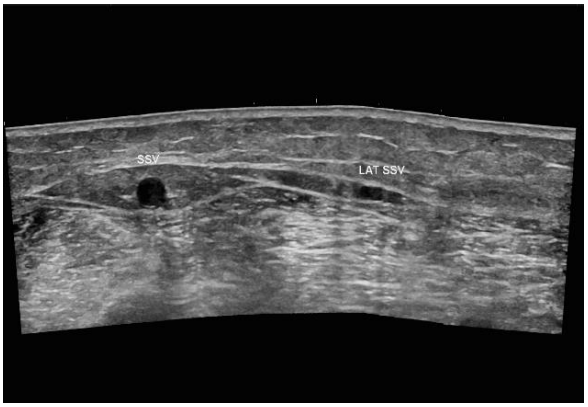


Image 22: Superficial peroneal nerve vein showing “string of beads” sonographpic appearance
Colour Doppler image of the superficial peroneal nerve vein (labelled as lateral SSV in the image) displays a "string of beads" (-reb-blue-red-) sonographic appearance.

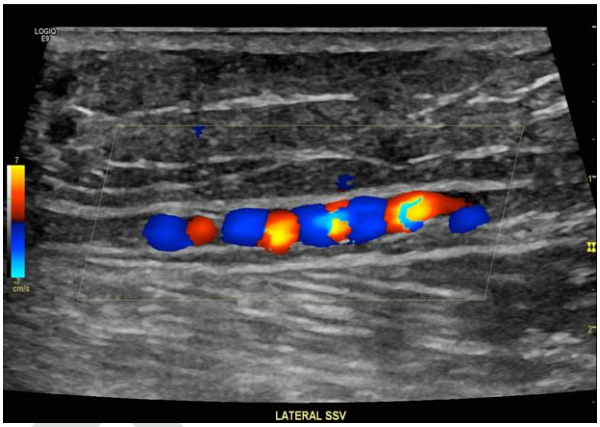


Image 23: Clinical image of the patient with varicosities in the posterolateral calf associated with an incompetent superficial peroneal nerve vein.

Image 24: Incompetent GSV
Colour and spectral Doppler imaging of the GSV with provocation manoeuvre. The sampled GSV segment demonstrates venous reflux upon the release of augmentation manoeuvre or diastolic phase following muscular contraction.

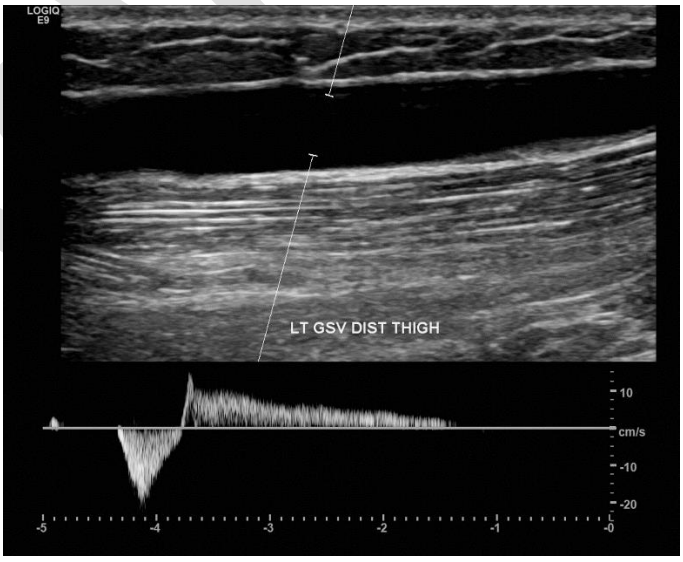

Image 25: Competent GSV.

Colour and spectral Doppler imaging of the GSV with provocation manoeuvre. The GSV demonstrates antegrade flow during distal augmentation manoeuvre and a brisk of physiological reversed flow on relaxation, indicating valvular competence in the samped GSV segment.

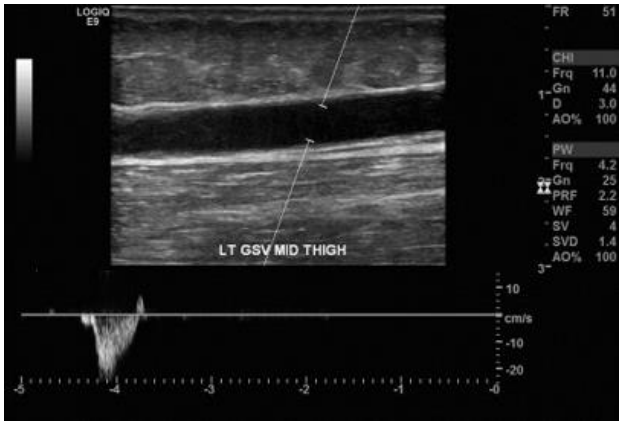


Image 26: Mickey mouse sign.

B-mode image of the left SFJ, mimicking a mickey mouse (Face: CFV; Right ear: GSV; Left ear: SFA).

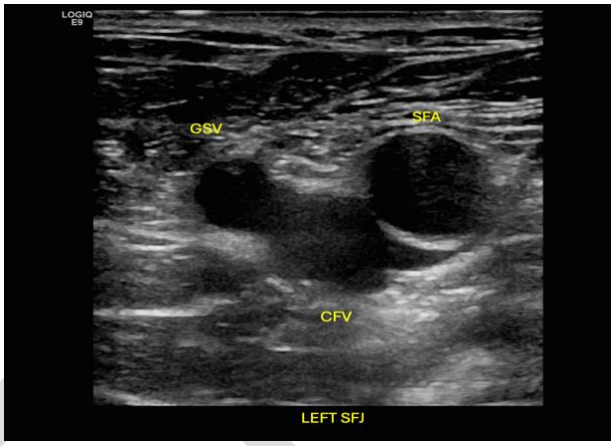


Image 27 : PW Doppler imaging of the CFV at the suprasaphenic and infrasaphenic levels.

Left image: With the sample gate placed above the level of the SFJ, the CFV demonstrates reflux flow on the release of augmentation manoeuvre. Right image: With the sample gate placed in the CFV segment below the SFJ, it appears competent with no apparent reflux flow detected, suggesting CFV incompetence is likely related to SFJ incompetence, and siphon effect of the GSV.

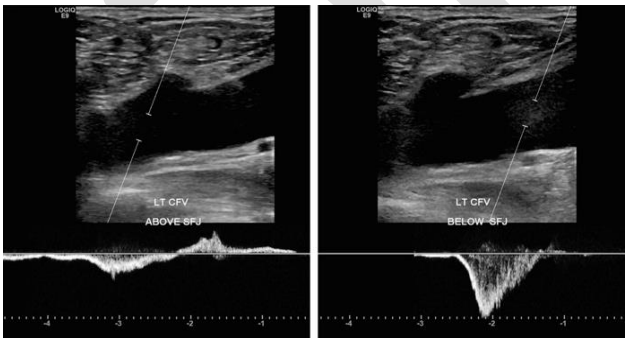


Image 28: Systolic reflux at the SFJ.

In the presence of obstructive disease in the ipsilateral iliofemoral veins, reversed flow (systolic reflux) is demonstrated at the right SFJ during provocation manoeuvre, that is further drained via collateral veins. Brisk reserved flow upon relaxation suggests competent terminal valves.

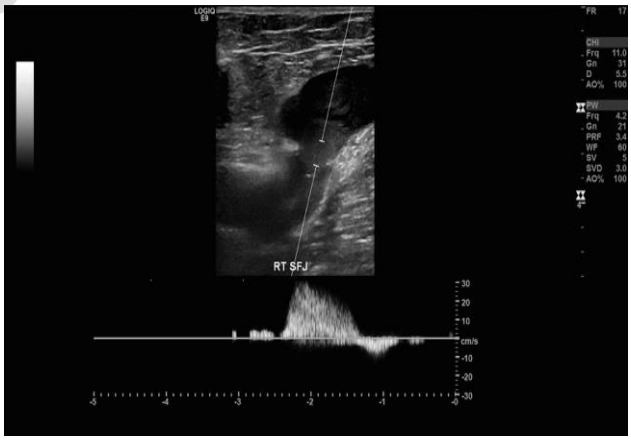

Image 29: Systolic and diastolic reflux at the SFJ.

Spectral and colour Doppler imaging of the left SFJ. When provocation manoeuvre is applied, augmented flow travels from the CFV back to the GSV via the SFJ, known as systolic reflux. The diastolic flow is also in a reversed direction of prolonged duration, suggesting valvular incompetence at the SFJ. The coexistence of systolic and diastolic reflux occurs secondary to venous obstruction in the ipilateral iliofemoral veins.

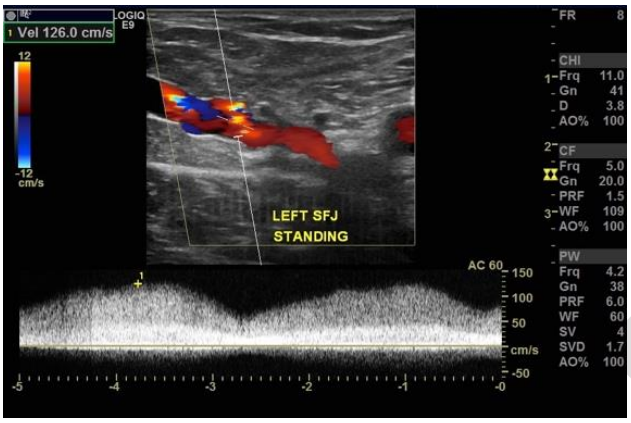


Image 30: Anatomical variant of the SFJ with the GSV crossing posterior to the SFA.

B-mode image of the right SFJ. The classic mickey mouse sign is not apparent; instead, the GSV joins the CFV on the lateral aspect after passing the SFA.

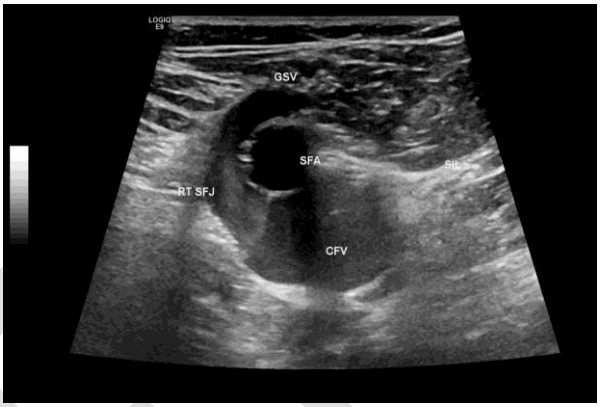


Image 31: Anatomical variant of the SFJ with the GSV passing through the gap between the SFA and PFA.

Colour Doppler image of the left SFJ shows the terminal section of the GSV is sandwiched by the SFA and PFA.

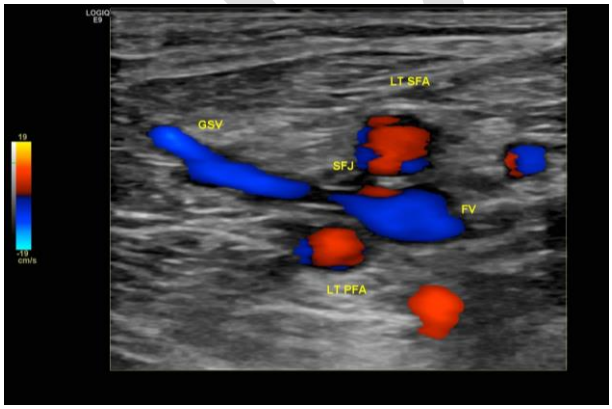


Image 32: Variable termination of the GSV (SFJ: GSV-FV).

Longitudinal B-mode image of the right SFJ shows the GSV terminates into the FV instead of the CFV.

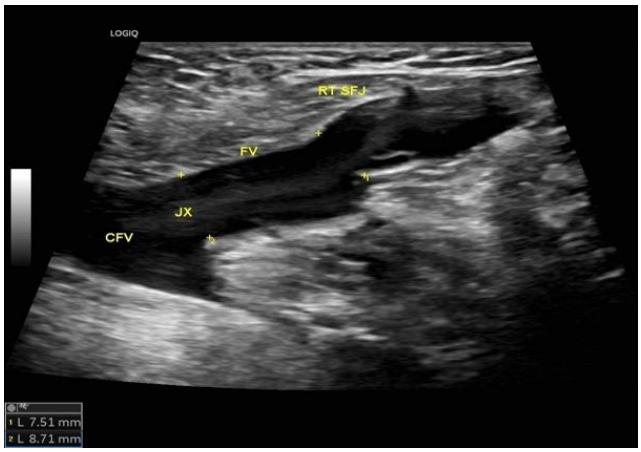

## Image 33: Variable termination of the GSV (SFJ: GSV-DFV).

Transverse B-mode image of the right SFJ shows the GSV terminates into the DFV instead of the CFV.

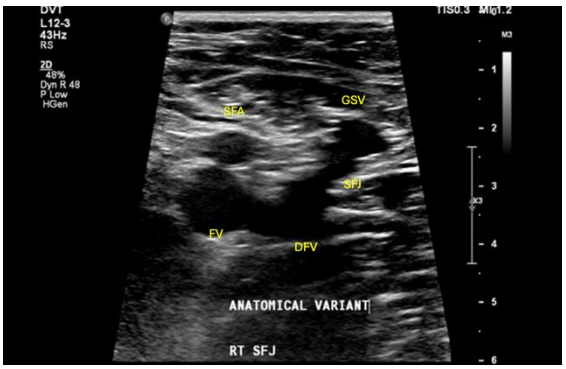


## Image 34: Saphenous pulsation.

At rest, the left GSV calf segment exhibits antegrade flow with a pulsatile pattern, indicative of saphenous pulsation. Notably, the spectral tracing shows no retrograde flow component, and the phenomenon is typically observed in patients with advanced stages of CVD/CVI, likely as a result of microcirculatory failure.

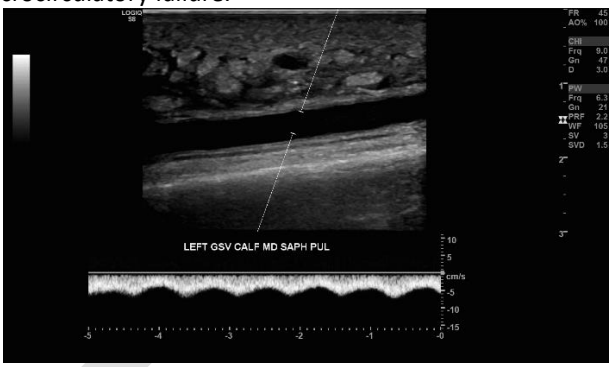


## Image 35: Continuous flow in the GSV.

At rest, the GSV demonstrates continuous antegrade flow due to venous obstruction in the femoropopliteal veins. Flow volume and velocity may increase when the patient lies in the supine position due to a reduction in the hydrostatic pressure gradient.

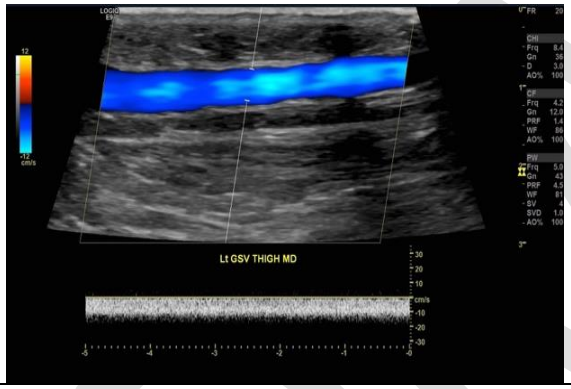


## Image 36: Varicocoele

Ultrasound image of varicocele shows dilated, tortuous veins within the scrotum, with increased echogenicity and noncompressibility, characteristic of a varicocele. The veins exhibit a "bag of worms" appearance, indicative of impaired venous drainage.

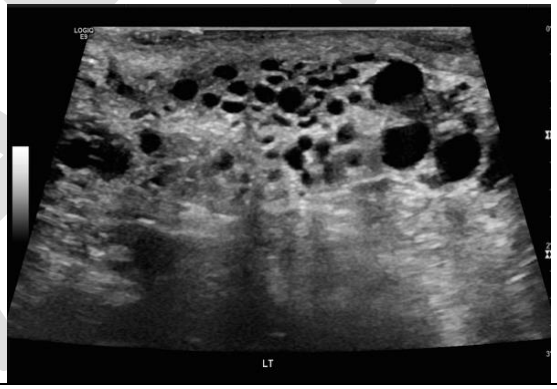


## Image 37: Systolic reflux at the SPJ.

During a provocation manoeuvre, augmented flow is observed traveling from the popliteal vein back to the SSV via the SPJ, indicating systolic reflux. However, upon relaxation, diastolic flow is absent on the spectral Doppler tracing, suggesting venous obstruction in the femoropopliteal vein and a competent SPJ.

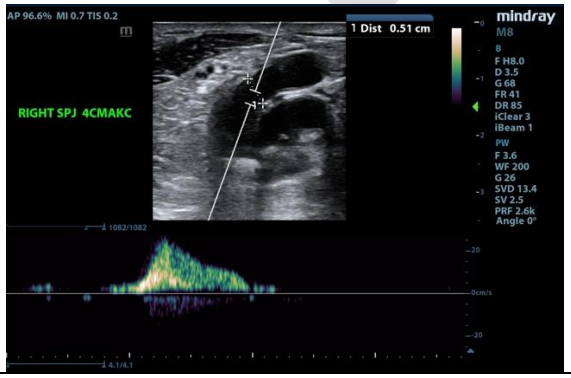


## Image 38: Systolic and disatolic reflux at the SPJ.

During a provocation manoeuvre, augmented flow travels from the popliteal vein back into the SSV via the SPJ. Diastolic flow is also reversed and prolonged, indicating SPJ incompetence. The co-occurrence of systolic and diastolic reflux is due to venous obstruction in the femoropopliteal vein.

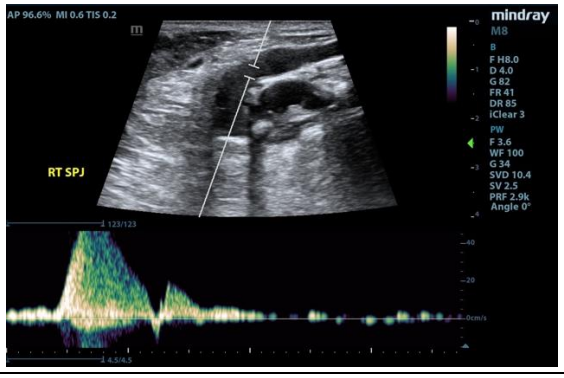

Image 39: Paradoxical reflux in the vein of Giacomini.

The left Giacomini's vein demonstrates flow in antegrade direction during both muscular systole and diastole. The diastolic flow most likely represents flow exiting out of the SPJ from the popliteal vein. This ascending reflux is known as paradoxical reflux.


Image 40: Competent perforating vein.

An ultrasound image of a competent posterior tibial perforating vein shows inward flow during augmentation and brisk reversed flow upon relaxaion (systolic: inward; diastolic: outward).

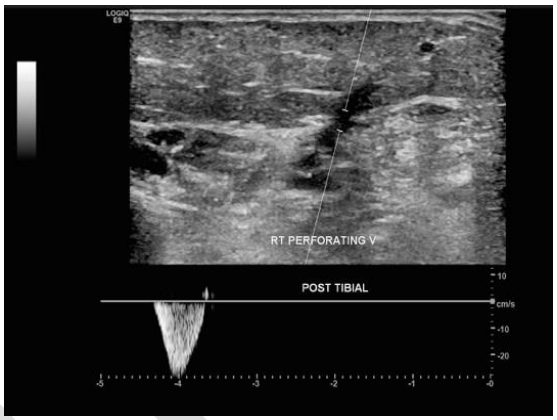


Image 41: Incompetent calf perforating vein.

The posterior tibial perforating vein shows inward flow during augmentation and reversed flow of long duration upon relaxation, indicating perforating vein incomeptence.

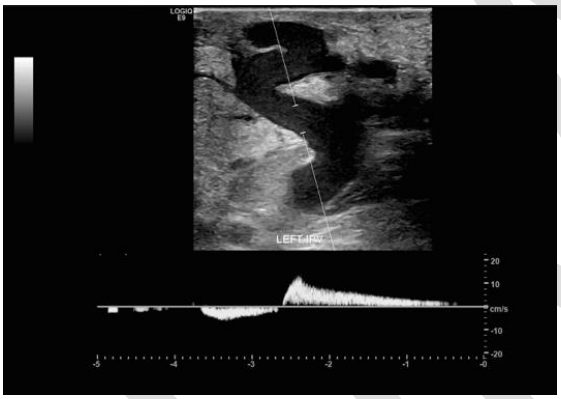


Image 42: Incompetent thigh perforating vein.

This thigh perforating vein is identified as the source of reflux responsible for recurrent thigh varicosities. During a provocation maneuver, the flow direction is inward, but upon relaxation, prolonged reversed flow is observed on the spectral tracing, indicating perforating vein incompetence.

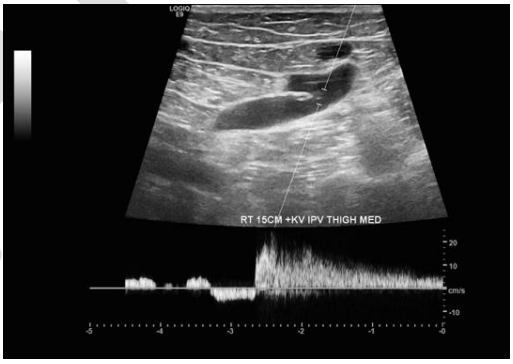


Image 43: Re-entry perforating vein with systolic and diatolic inflow.

The lateral calf perforating vein demonstrates inward flow during and after augmentation (systolic: inward; diastolic: inward). This perforator functions as a re-entry point, draining superficial venous reflux.

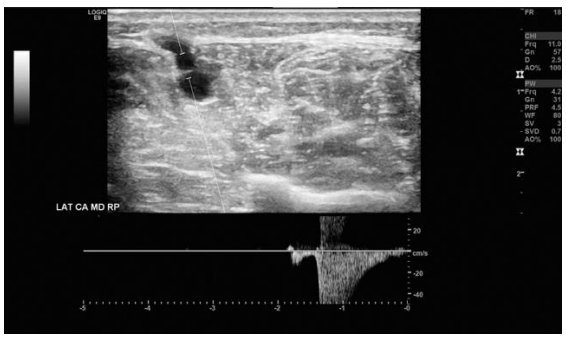


Image 44: Incompetent perforator with systolic inflow and diastolic outflow.

The mid thigh perforating vein demonstrates inward flow during augmentation and outward flow upon relaxation (systolic: inward; diastolic: outward). This thigh perforating vein is identified as the source of reflux or an escape point.

Image 45: Re-entry perforating vein with systolic outflow and diastolic inflow.

The medial calf perforating vein shows outward flow during augmentation and inward flow upon relxation (systolic: outward; diastolic: inward). This perforating vein functions as a re-entry point; however, systolic flow suggests the possibility of deep vein obstruction or incompetence.

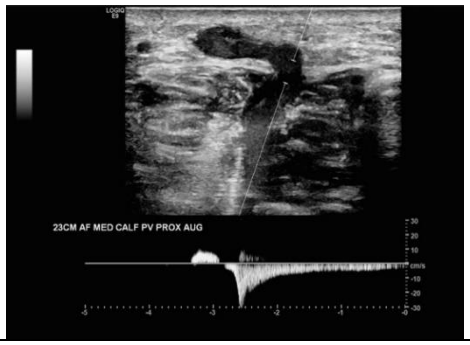


Image 46: Incompetent perforator with systolic and diastolic outflow.

The paratibial perforating vein shows outward flow during and after augmentation manoeuvre (systolic: outward; diastolic: outward). This perforating vein is defined as the source of reflux or escape point. Addtionally, its systolic flow suggests the possibility of deep vein obstruction or incompetence.

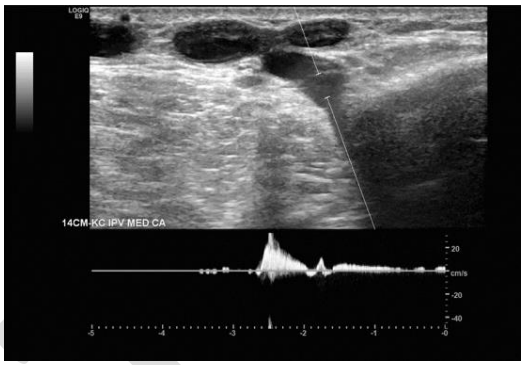


Image 47: Vulval varicosties.

B-mode image of a patient with right sided vulval varicosities.

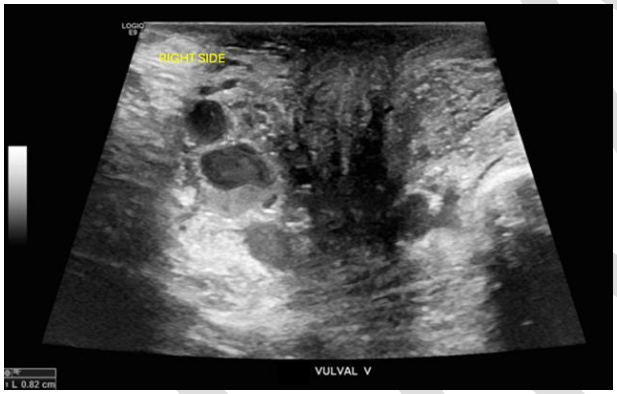


Image 48: Clinical image of a patient with gluteal varicosities.

Image 49: Gluteal perforating vein.

PW Doppler analysis of this gluteal perforating vein shows minimal inward flow during augmentation and reversed flow of prolonged duration on the release of augmentation manoeuvre, indicating perforating vein incompetence.

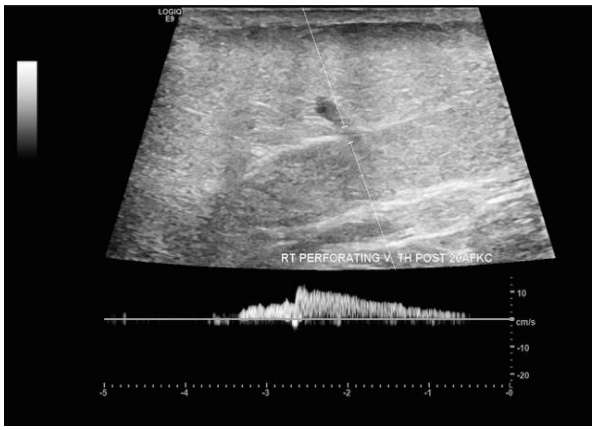


Image 50: Clinical image of popliteal fossa vein.

Image 51: Popliteal fossa perforating vein.

PW Doppler imaging of the popltieal fossa perforating vein shows inward flow during muscular contraction followed by high velocity, high volumed reflux flow upon relaxation.

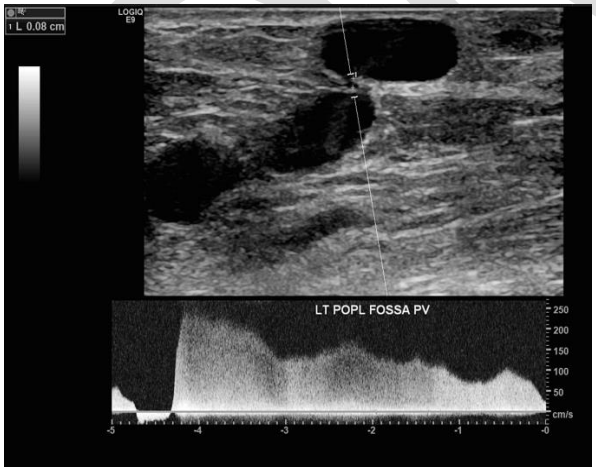


Image 52: Clinical image of a patient with large varicosities on the posterolateral aspect of the thigh.

Image 53: Posterolateral thigh perforating vein.
PW Doppler imaging of the left lateral thigh perforating vein shows inward flow (superficial to deep) during augmentation and outward flow (deep to superficial) of prolonged duration, indicating perforating vein incompetence.

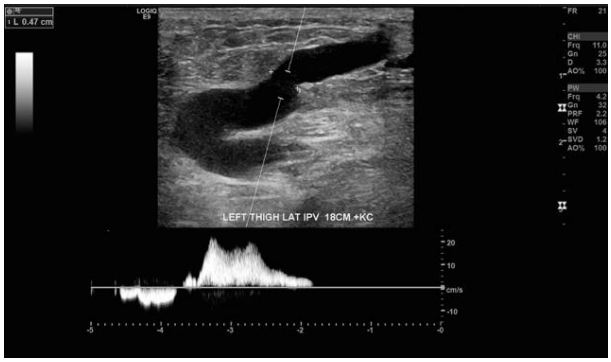


Image 54: Clinical image of a patient with varicose veins on the lateral aspect of the calf attributed to incompetent sciatic nerve varices.

Image 55: SNV
PW Doppler imaging of sciatic nerve varices shows antegrade flow during augmenatation and reversed flow of prolonged duration on relaxation.

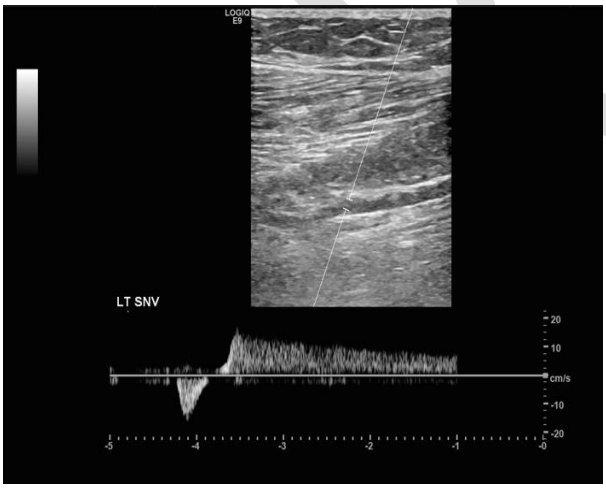


Image 56: Clinical image of a patient with an incompetent knee perforating vein, contributing to varicosities on the knee and the anterior aspect of the calf.

Image 57: Incompetent knee perforating vein.
PW Doppler imaging of a knee perforating vein shows reflux flow during muscular contraction and relaxation, indicating perforating vein incompetence.

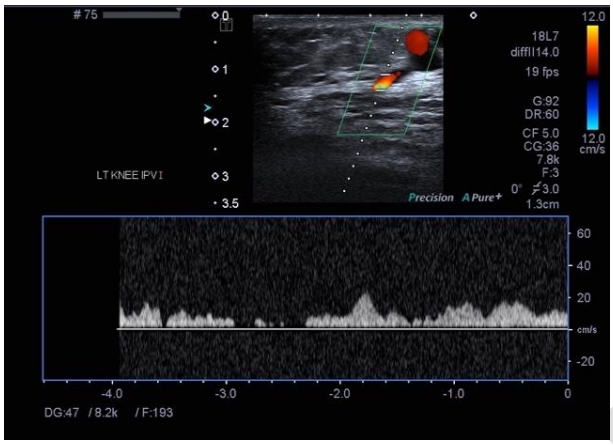


Image 58: Clinial image of a patient with bilateral incompetent bone perforating veins.

Image 59: Bone perforating vein.
B-mode image of a bone perforating vein shows a small ostelytic defect on the tibial shaft with diameter 0.6mm.


Image 60: Clinical image of a patient with the LNVN, contributing varicosities on the anterolateral aspect of the thigh.

Image 61: Incompetent LNVN.

PW Doppler imaging of the LNVN shows augmented flow in antegrade direction and reflux flow on relaxation.

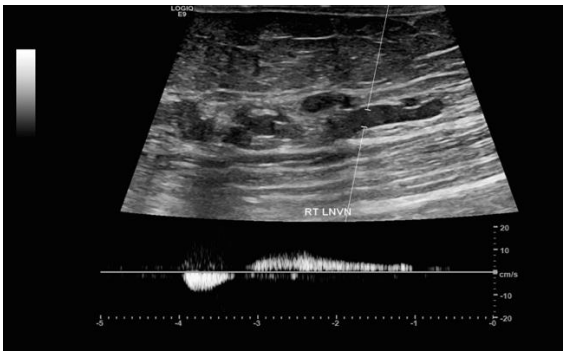


Image 62: Ablated GSV following EVLA.

PW and colour Doppler imaging shows absence of flow signals in the GSV thigh segment that has undergone EVLA treatment.

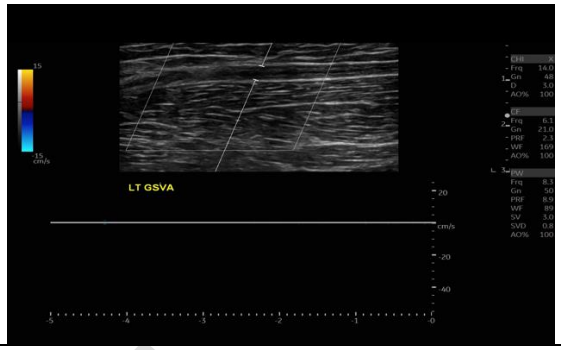


Image 63: The GSV following cyanoacrylate glue ablation.

B-mode image of the GSV shows acoustic shadowing caused by the cyanoacrylate glue.


Image 64: Strip-track haematoma post-GSV stripping surgery.

Postoperative image of the saphenous compartment showing strip-track haematoma following GSV stripping surgery.

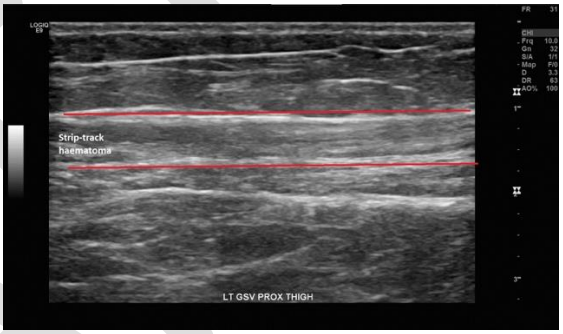


Image 65: SFJ post high ligation.

Postoperative image of the former SFJ following flush ligation.

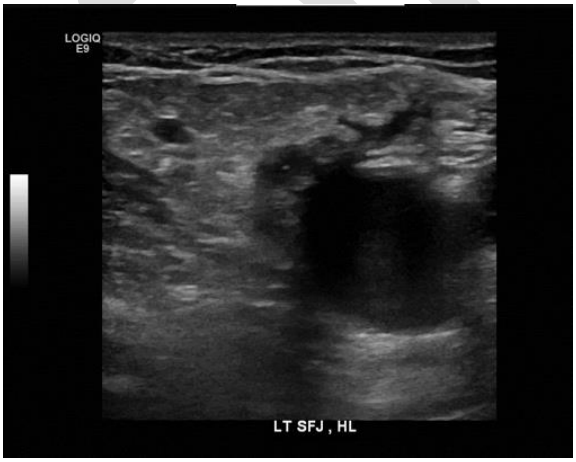


Image 66: SFJ with a GSV stump post ligation.

Postoperative image of the left SFJ following low ligation with a residual GSV stump.

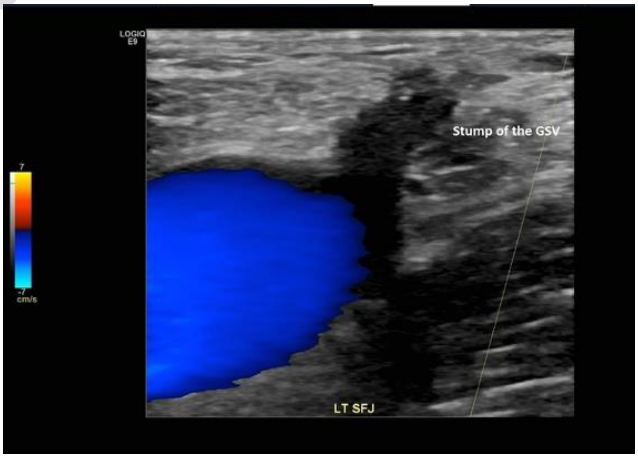

Image 67: STP postavulsion.

Ultrasound image of an avulsed thigh tributary vein with superficial venous thrombosis and absence of vascularity.


Image 68: Type I EHIT.

Type I EHIT where the thrombosis stops at the SFJ.

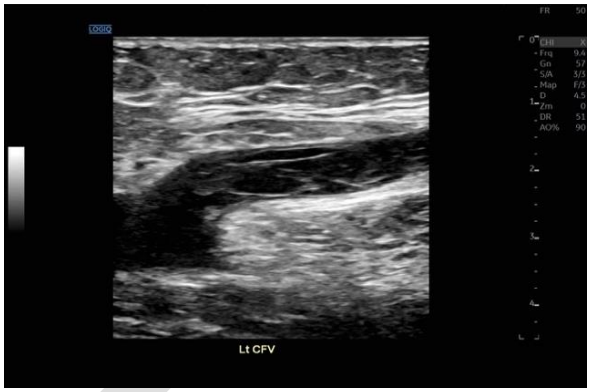


Image 69: Type II EHIT.

Type II EHIT where the thrombus extends into the CFV causing less than 50% of luminal reduction.

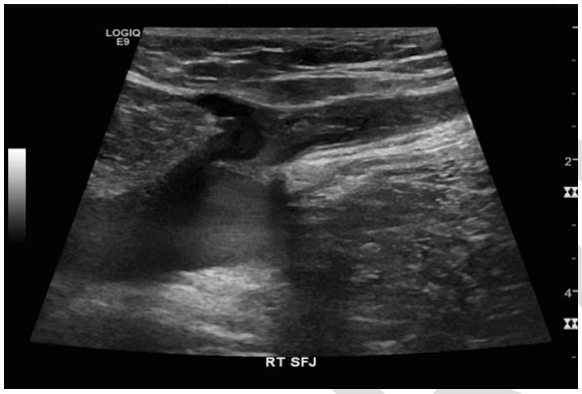


Image 70: Type III EHIT.

Type III EHIT where the thrombus extends into the CFV causing greater than 50% of luminal reduction.


Image 71: Type IV EHIT.

Type IV EHIT where the thrombus extends into the CFV causing complete occlusion of the CFV.

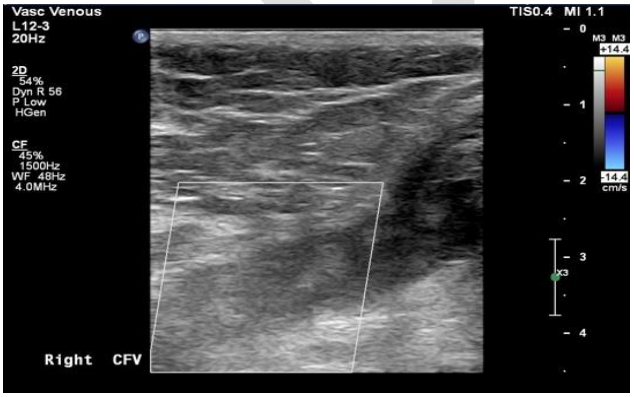


Image 72: Mobile EHIT.

B-mode image displaying a mobile type of endovenous heat-induced thrombosis (EHIT) reveals a flap at the SFJ following an endovenous laser ablation procedure.

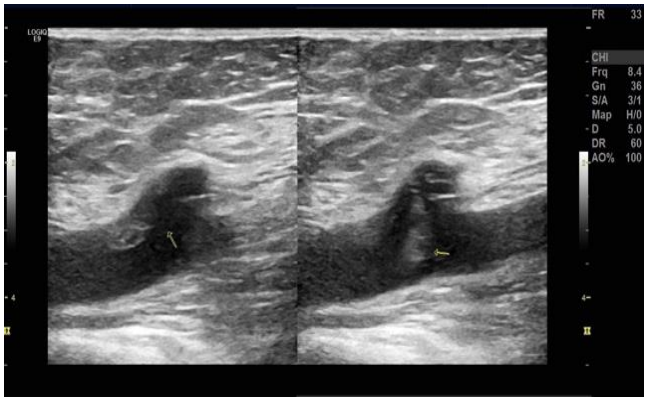

Image 73: EGIT.

Extension of the glue into the left popliteal vein following cyanoacrylate glue ablation of the SSV.

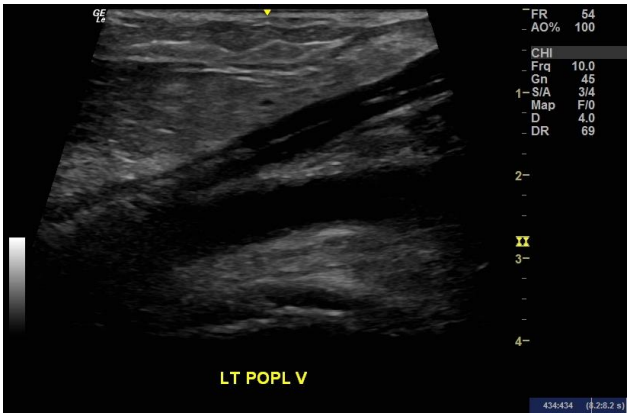


Image 74: DVS.

Deep vein sclerosae (DVS). After the injection of medial calf tributary veins with 3% 1-5 foam sodium tetradecyl sulfate, deep vein sclerosae or deep vein fibrosis is present in the posterior tibial perforator located at 8cm above the level of medial malleoli, extending into the posterior tibial veins. The veins with deep vein sclerosae appear to have similar appearance to those with deep vein thrombosis with internal echogenicity.

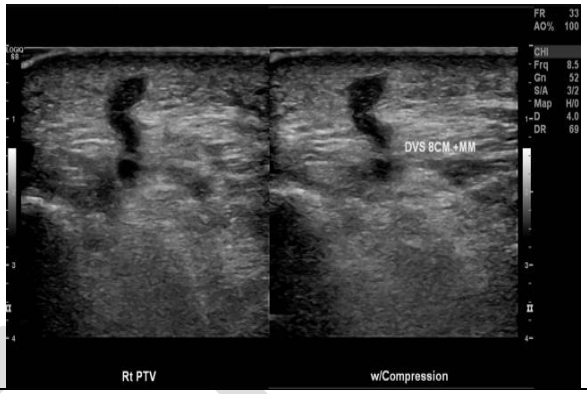


Image 75: STP.

An acute superficial thrombus spontaneously formed in the large varicose tributary vein, showing internal hypoechogenicity.


Image 76: Seroma.

Ultrasound image of an inguinal seroma that is formed after the SFJ ligation and stripping of the GSV.

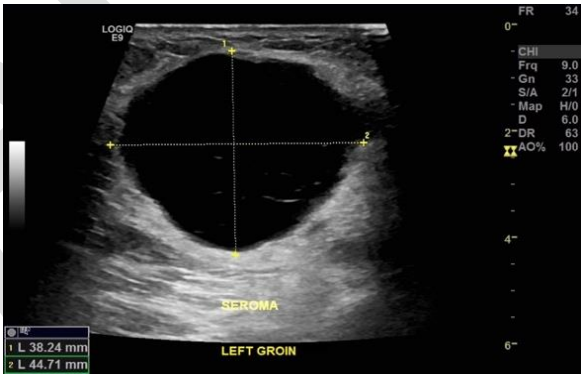


Image 77: Haematoma.

Ultrasound image showing a large, well defined, oval-shaped haematoma formed after SFJ ligation. It has a multi-laminated, whorled appearance in the anterior region and a fluid component along the posterior wall.

Image 78: Sural nerve injury post EVLT.

Ultrasound image of an iatrogenic injury to the sural nerve resulting from an SSV ablation procedure, showing a thickened nerve and partial loss of the fascicular pattern.

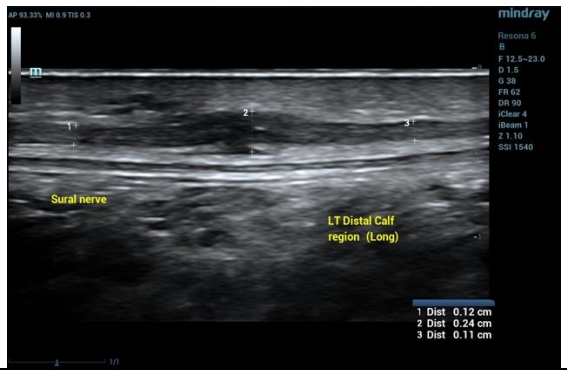

Image 79: Cutaneous necrosis.

Cutaneous necrosis after injection with polidocanol 1% into telangiectasia. Superficial ulceration is present on the anterior aspect of the calf at week 2.

Image 80: Membranous fat necrosis.

Ultrasound image of fat necrosis as a result of extravasation of sclerosant into the subcutaneous adipose tissue.

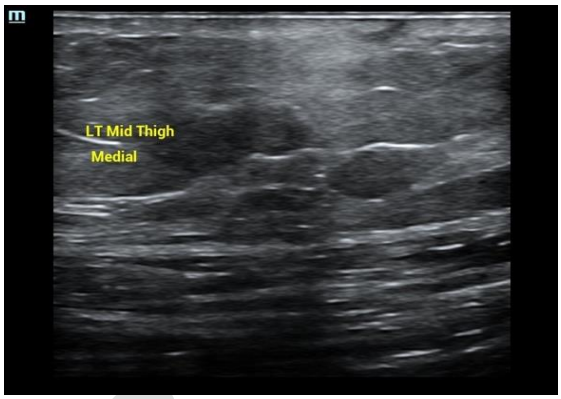


Image 81: Neovascularisation post ELVA.

Spectral and colour Doppler image shows neovascularisation within a previously ablated GSV with arterialised venous flow in retrograde direction flushing the treated segment.

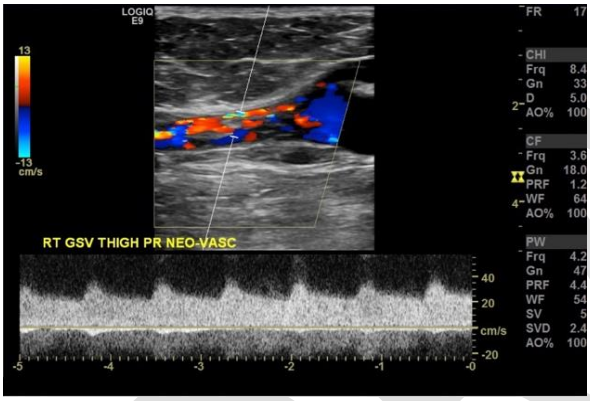


Image 82: Iatrogenic AVF.

Iatrogenic AVF. The left SFJ exhibits arterialised venous flow of high velocity and high volume due to arteriovenous fistula caused by needle injury during the administration of tumescence anaesthesia.

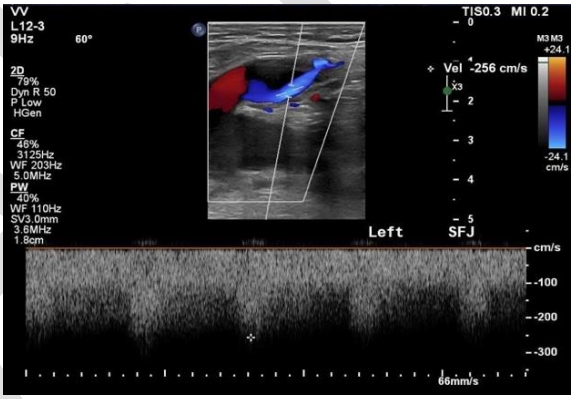


Image 83: Clinical image of the Type IV hypersensitivity in a patient who had endovenous cyanoacrylate glue ablation of the GSV.

Image 84: Granuloma.

B-mode image of a granuloma at the venous access site following cyanoacrylate glue ablation shows an irregularly shaped lesion with heterogeneous echogenicity and acoustic shadowing cast by the glue.

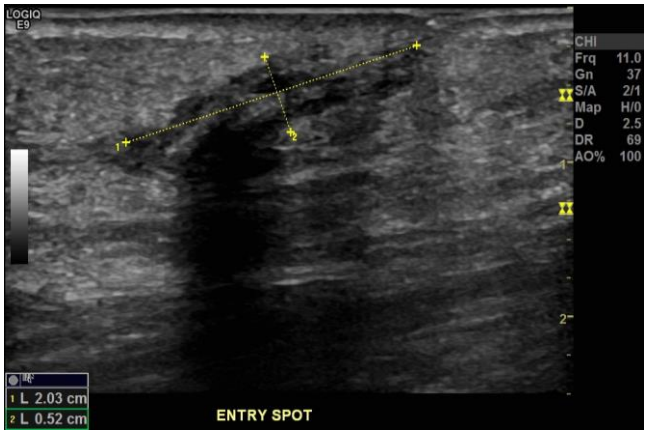

Image 85: Cellulitis.

Ultrasound of the left leg with cellulitis shows hyperechoic fat lobules separated by hypoechoic fluid filled areas, commonly referred to as a "cobblestone" appearance.

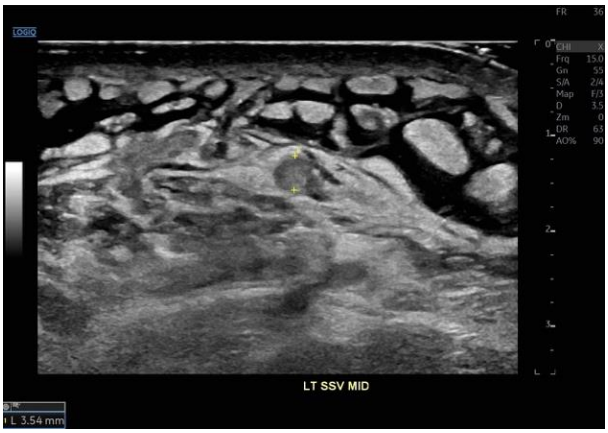


Image 86: Clinical image of a patient with leg lymphoedema.

Image 87: Lymphodema.

Ultrasound image of a patient with lymphedema shows thickened subcutaneous tissue with increased echogenicity, accompanied by multiple hypoechoic areas representing fluid accumulation, characteristic of lymphedema.

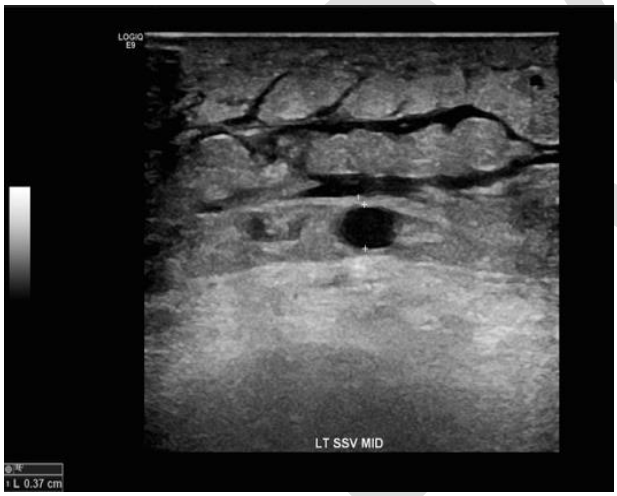


Image 88: Clinical image of the patient's legs with lipodema.

Image 89: Lipodema.

Ultrasound image of the patient's leg with lipedema shows thickened subcutaneous fat.

Image 90: Lipoma.

Ultrasound image of a lipoma shows a well-defined, hyperechoic mass within the subcutaneous tissue, with homogenous texture and smooth margins, consistent with the benign characteristics of a lipoma.

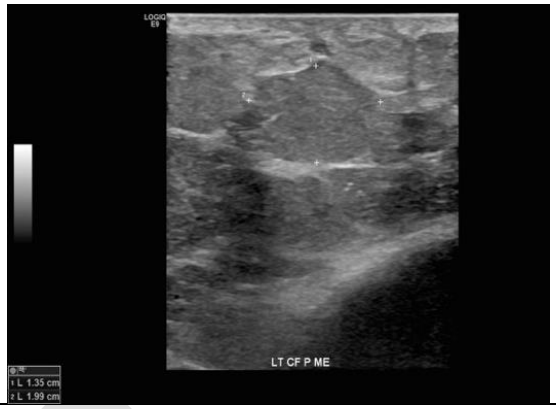


Image 91: AVM.

Ultrasound image of an AVM on the the right forefoot shows low resistive arterial flow within the area of intrest.

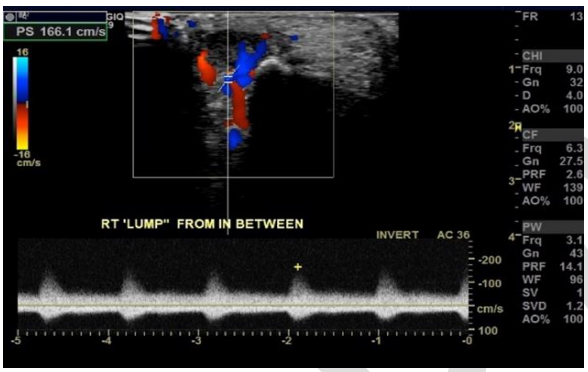


Image 92: Venous malformation.

B-mode ultrasound image of an intramuscular venous malformation at the posterior thigh shows tubular, sponge like spaces within the muscle, with no evidence of thrombi.


Image 93: Muscle hernia.

Ultrasound image of a muscle hernia shows a focal defect in the fascia, through which a portion of the underlying muscle protrudes. The herniated muscle appears as a hypoechoic mass extending through the fascial defect, especially prominent during muscle contraction.

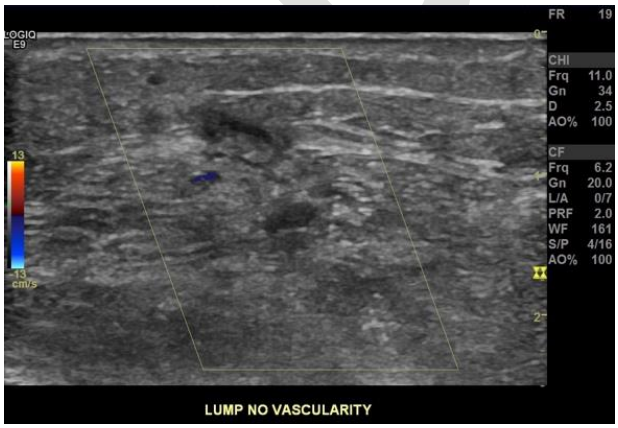


Image 94: Baker’s cyst.

Ultrasound image of a baker's cyst with internal echgenic material suggestive of an old haemorrhage.

Image 95: Neuroma.
Ultrasound image of a stump neuroma shows a hypoechoic, well circumscribed mass at the site of a nerve stump.

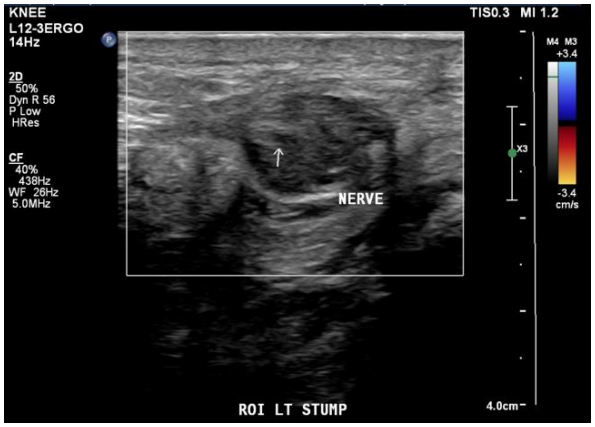


Image 96: Clinical image of a patient with Klippel Trenaunay syndrome.

Image 97: Transmitted pulsatility in the CFV.
PW Doppler imaging of the right CFV shows spontaneous flow with pulsatile retrograde flow, suggesting a possible right sided heart problem.

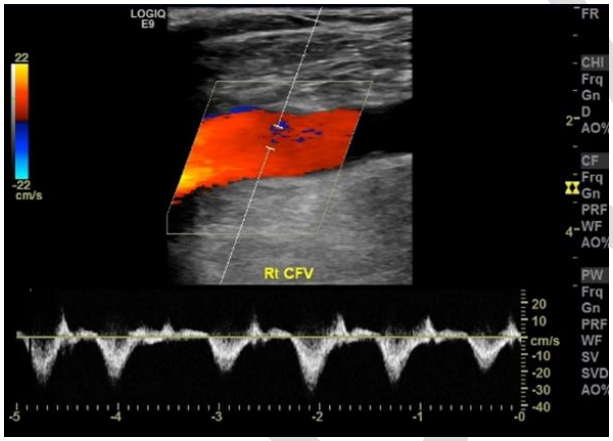


Image 98: Transmitted pulsatility at the SFJ.
PW Doppler imaging of the left SFJ reveals pulsatile reversed flow that mimics venous reflux, indicating a possible right sided heart problem.

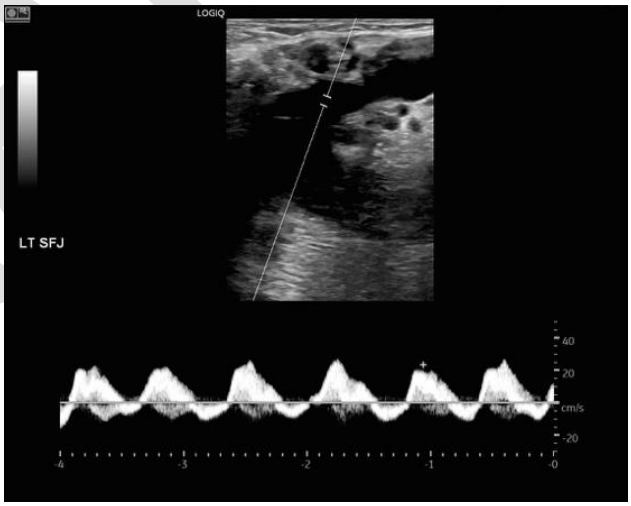

| Room setups | |
|---|---|
| Image 99: Room setup with a titable couch.<br> 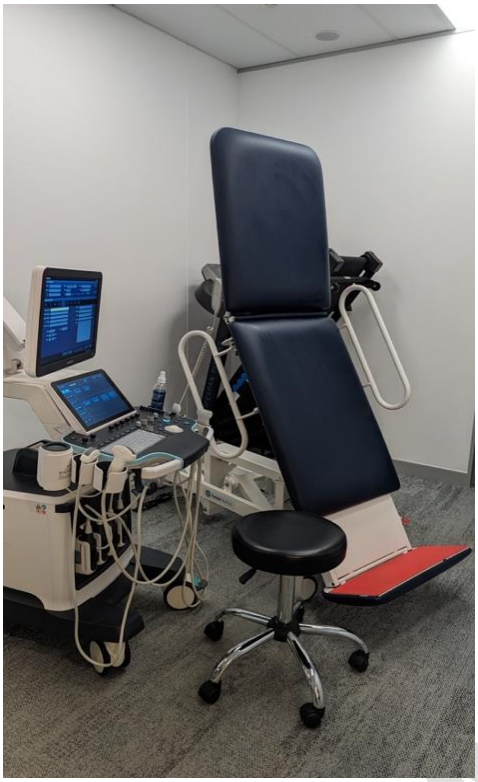 | Image 100: Room setup with a titable couch and an external monitor.<br>  |
| Image 101: Room setup with a height adjustable couch, two step stool, low chair and an external monitor.<br> 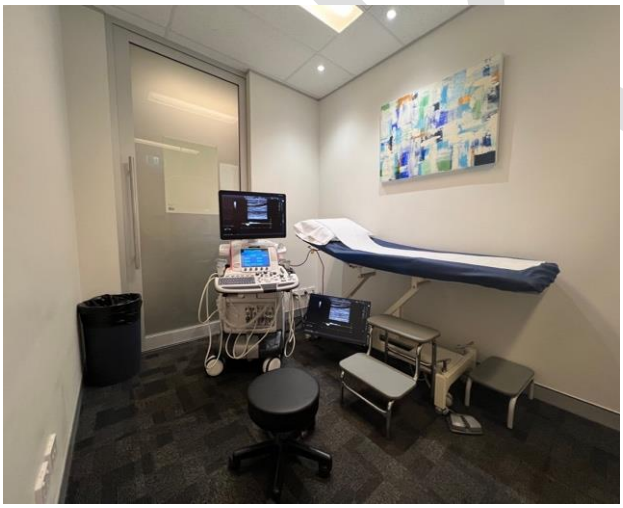 | Image 102: Room setup with a height adjustable couch, two step stool, yoga ball and an external monitor.<br> 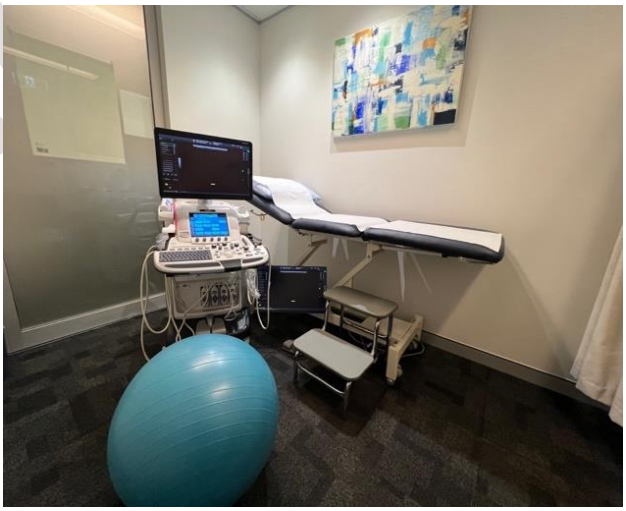 |